Research on Engineering Structures & Materials
www.jresm.org
Research Group

Research Article

Flexural behavior of reinforced concrete beams incorporating fly ash, GGBS, and Alccofine

Lokala Hari RamaKrishna [*,1,a], A Venkateswara Rao [1,b], Komma Hemanth Kumar Reddy [2,c], S Jyothirmayee [3,d], Bhanu Prakash Twarakavi [4,e]

[1]*Department of Civil Engineering, Koneru Lakshamiah Educational Foundation, Vaddeswaram, Guntur District, 522302, India*
[2]*Department of Civil Engineering, K S R M college of engineering, Kadapa District, 516003, India*
[3]*Department of Civil Engineering, JNTUA college of engineering, Pulivendula, Kadapa District, 516390, India*
[4]*Department of Civil Engineering, PBR Visvodaya institute of technology and science, Kavali, Nellore District, 524201, India*

Article Info

Article History:

Received 23 Feb 2026
Accepted 08 May 2026

Keywords:

Ternary composite concrete;
Fly ash;
Ground granulated blast furnace slag;
Alccofine;
Flexural performance;
Sustainable concrete

Abstract

The increasing demand for low-carbon concrete necessitates the development of binder systems that are capable of simultaneously ensuring structural performance and sustainability. This study presents an experimental investigation on the mechanical, structural and microstructural behavior of M30 grade concrete incorporating ternary blended binders composed of fly ash, ground granulated blast furnace slag and Alccofine. A systematic replacement strategy was adopted to identify an optimal binder composition that balances strength development and material efficiency. Mechanical properties were evaluated at 7 and 28 days, while reinforced concrete beams were tested under loading to assess load-deflection response and crack development. Microstructural analysis using scanning electron microscopy and energy dispersive X-ray analysis was performed to examine hydration morphology and interfacial transition zone characteristics. The results indicate that the optimized ternary mix achieved improvements of 19.29% in compressive strength, 33.3% in split tensile strength and 33.85% in flexural strength compared to the control mix. Structural testing showed enhanced load-carrying capacity, improved deformation response and delayed crack propagation. The findings suggest that the combined effect of particle packing, secondary hydration and interfacial transition zone refinement contributes to improved tensile behavior. In addition, the optimized mix achieved 52% clinker reduction, demonstrating its potential for sustainable structural applications.

1. Introduction

The extensive use of cement as the primary binder in reinforced concrete construction poses significant challenges in terms of sustainability, durability, and long-term structural performance [1-3]. Cement production is among the most energy-intensive industrial processes involving high-temperature clinkerization and the inevitable release of carbon dioxide during limestone decarbonation [4,5]. As a result, the cement industry accounts for approximately 7–8% of global anthropogenic CO_2 emissions, prompting increasing regulatory and research-driven efforts to reduce OPC consumption in structural concrete [6-8]. In addition to its environmental burden, OPC-dominant concrete is frequently associated with durability-related concerns, including drying

*Corresponding author: harilokala17@gmail.com
[a]orcid.org/0009-0008-2128-1610; [b]orcid.org/0000-0002-9472-7846; [c]orcid.org/0000-0002-4353-3072; [d]orcid.org/0000-0002-0653-4383; [e]orcid.org/0009-0006-8911-3360
DOI: http://dx.doi.org/10.17515/resm2026-1529me0223rs

shrinkage, early-age microcracking, and vulnerability to aggressive exposure conditions such as chloride ingress, sulphate attack, and carbonation, all of which compromise serviceability and long-term structural performance [9-11]. Partial replacement of ordinary Portland cement (OPC) with supplementary cementitious materials (SCMs) has emerged as an effective strategy for improving sustainability, mechanical performance and durability of concrete [12-14]. Among widely used SCMs fly ash and ground granulated blast furnace slag (GGBS) have been extensively investigated and implemented in structural concrete applications [15,16]. Fly ash, a siliceous and aluminous by-product of coal-fired power generation contributes primarily through pozzolanic reactions by consuming calcium hydroxide released during cement hydration to form secondary calcium silicate hydrate (C–S–H) and calcium aluminosilicate hydrate phases [17-19]. These reactions refine pore structure, reduce permeability, and enhance long-term strength and durability [20,21]. In addition, the substantially spherical morphology of fly ash particles improves fresh-state workability by enhancing particle distribution and reducing internal friction [22,23]. GGBS, produced by rapid quenching and grinding of molten blast furnace slag, exhibits latent hydraulic behavior and contributes additional binding phases under alkaline conditions, resulting in a denser cementitious matrix and improved resistance to chloride ingress and sulphate attack [24-26]. Despite these advantages, binary cementitious systems incorporating fly ash or GGBS exhibit certain limitations, particularly at higher replacement levels [27]. High-volume fly ash concretes often suffer from slower hydration kinetics and reduced early age strength development limiting their relevance in structural members requiring early stiffness and load carrying capacity [28,29]. Similarly excessive replacement of OPC with GGBS may extend setting time and delay early heat evolution, adversely affecting early mechanical performance despite alterations in long-term durability [30,31]. These limitations are especially critical for commonly adopted design grades such as M30, where a balance between early-age strength development, long-term durability, and structural reliability is required [32].

To overcome the limitations of conventional binary blends, recent research has progressively focused on ternary cementitious systems incorporating ultrafine and highly reactive mineral additives [33,34]. Among these, Alccofine-1203 an ultrafine slag-based mineral admixture with high fineness and reactive aluminosilicate content has gained consequential attention for its ability to modify hydration kinetics and microstructural evolution [35-37]. Unlike traditional SCMs that contribute primarily through slower pozzolanic or latent hydraulic reactions. Alccofine plays a dual role within the cementitious matrix physically acting as a micro-filler to enhance particle packing density and chemically providing nucleation sites that accelerate early hydration and promote rapid C–S–H formation [38-40]. These mechanisms lead to refinement of the interfacial transition zone (ITZ) improved phase continuity and enhanced early age strength development [41,42]. The combined fusion of fly ash, GGBS, and ultrafine Alccofine in ternary blended cementitious systems enables complementary physical and chemical interactions [1]. Fly ash contributes to long-term microstructural refinement through sustained secondary hydration, GGBS enhances durability through latent hydraulic binding, and Alccofine improves early-age densification through packing optimization and hydration acceleration [43,44].

The combined use of these materials produces a more homogeneous and compact microstructure with reduced pore interaction and improved load transfer pathways which enhances compressive strength and improves tensile and flexural performance by delaying microcrack initiation and enabling improved stress redistribution under applied loading [37,45,46]. Although numerous studies have examined the mechanical and durability performance of binary and ternary SCM-based concretes, much of the existing literature remains focused on material-level characterization, particularly compressive strength and durability indices [10,37]. Comparatively limited attention has been directed toward establishing explicit relationships between microstructural evolution and the structural behavior of reinforced concrete members [10,47]. In practice, the performance of reinforced concrete beams is governed by cracking behavior, stiffness degradation, load–deflection response, and failure modes, which cannot be fully captured through specimen-scale testing alone [10,48,49]. However, existing studies predominantly focus on material-level properties such as compression strength and durability indices, with limited emphasis on establishing a direct and experimentally validated relationship between microstructural

refinement and member-level structural response, particularly in terms of load- deflection behavior, cracking characteristics and stiffness degradation of reinforced concrete beams [50- 52].

Despite extensive studies on supplementary cementitious materials, most existing research is limited to material-level characterization, with insufficient emphasis on establishing a direct and experimentally validated relationship between microstructural evolution and structural behavior of reinforced concrete members [53-58]. In this context, the present study introduces a multi-scale experimental framework that quantitatively links ternary binder composition, microstructural refinement, and flexural performance of reinforced concrete beams [59]. Unlike previous studies, this work integrates mechanical testing, beam-level structural response, and microstructural evidence to establish a direct correlation between hydration mechanisms, interfacial transition zone characteristics, and load–deflection behavior [60-62]. This approach provides a more comprehensive understanding of how binder-level modifications influence structural performance [63-66].

2. Materials

2.1 Constituent Materials

The use of Ordinary Portland Cement (OPC, 53 grade) was considered as the main binding agent. Class F fly ash, Ground Granulated Blast Furnace Slag (GGBS), and Alccofine-1203 were considered as supplementary cementitious materials to prepare ternary binder mixes. All the materials were considered in their as-presented form without any further processing. OPC contributed to early strength development and creating an alkaline environment in the pores to facilitate the subsequent hydration reactions. The addition of supplementary materials was done to enhance the late strength and facilitate the pore refinement of the hardened mass. The physical properties of the component materials are given in Table 1, and the oxide contents are given in Table 2. Fly ash meets IS 3812 (Part 1):2013[53] specifications, and GGBS meets IS 12089:1987 [54] specifications. The supplementary distribution of SiO_2, Al_2O_3, and CaO-rich phases helps in the combined pozzolanic and latent hydraulic reactivity. The physical appearance and particle characteristics of materials are shown in Fig. 1(a–c). Fly ash consists of fine, rounded particles, which improve workability and exhibit delayed pozzolanic activity. GGBS appears as finer, irregular-shaped particles with latent hydraulic properties under alkaline conditions.

Table 1. Summary of the physical properties of the constituent materials used in this study

Material	Specific gravity	Bulk density (kg/m^3)
Cement (OPC)	3.01	1440
GGBS	2.85	1300
Fly ash	2.28	979
Alccofine	2.70	680
Fine aggregate	2.62	1600
Coarse aggregate	2.66	1550

Alccofine contains ultrafine particles that promote heterogeneous nucleation and enhance particle packing in the binder matrix. The combination of these components promotes staged hydration reactions and results in a gradual refinement and densification of the cementitious matrix.

(a) (b) (c)

Fig. 1. Physical appearance of cementitious materials; (a) GGBS (100 µm), (b) fly ash (50 µm) and (c) Alccofine (20 µm)

Table 2. The chemical composition of the cementitious materials used in this study.

Oxide	Cement	Fly Ash	GGBS	Alccofine
SiO_2	18.7	54.22	34.06	35.03
Al_2O_3	4.5	31.18	20.00	21.4
CaO	64.8	1.35	32.6	32.20
Fe_2O_3	4.1	2.63	0.8	1.20

2.2 Mix Proportioning

The concrete mix design was done to produce M30 grade concrete as per IS 10262:2019 [55], with the control mix designed using Ordinary Portland Cement. To investigate the influence of ternary hybrid cementitious materials cement was partially replaced with fly ash, GGBS and Alccofine following a systematic replacement strategy while maintaining consistent workability and strength requirements. Fly ash content was varied up to 25%, GGBS content ranged between 15% and 35%, and Alccofine was incorporated in the range of 10% to 12% by weight of total binder. The selected replacement ranges for fly ash, GGBS, and Alccofine were based on previous studies and preliminary trials to ensure a balance between early-age strength development, workability and long-term hydration, while avoiding excessive dilution of clinker content that could adversely affect structural performance. For all mixes, the total binder content was kept constant to isolate the effect of material replacement on performance. The detailed percentage proportions of OPC, fly ash, GGBS and Alccofine adopted for each mix are presented in Table 3. A total of ten mix proportions including one control mix and nine blended mixes were designed and evaluated to identify optimum combinations based on mechanical properties.

Table 3. Mix proportions of concrete mixes incorporating ternary blended binders

Mix ID	Cement kg/m^3	Fly Ash kg/m^3	GGBS kg/m^3	Alccofine kg/m^3	Coarse Aggregate kg/m^3	Fine Aggregate (kg/m^3)	Water (kg/m^3)	W/B Ratio	Cement (%of Binder)	Fly Ash (%of Binder)	GGBS	Alccofine (% of Binder)	Total SCMs (% of Binder)
M1	380.0	0.0	0.0	0.0	1308	555	177	0.466	100.0%	0.0%	0.0%	0.0%	0.0%
M2	190.0	76.0	76.0	38.0	1308	555	177	0.466	50.0%	20.0%	20.0%	10.0%	50.0%
M3	163.4	95.0	76.0	45.6	1308	555	177	0.466	43.0%	25.0%	20.0%	12.0%	57.0%
M4	133.0	95.0	114.0	38.0	1308	555	177	0.466	35.0%	25.0%	30.0%	10.0%	65.0%
M5	125.6	95.0	114.0	45.6	1308	555	177	0.466	33.0%	25.0%	30.0%	12.0%	67.0%
M6	152.0	95.0	95.0	38.0	1308	555	177	0.466	40.0%	25.0%	25.0%	10.0%	60.0%
M7	106.4	95.0	133.0	45.6	1308	555	177	0.466	28.0%	25.0%	35.0%	12.0%	72.0%
M8	182.4	76.0	76.0	45.6	1308	555	177	0.466	48.0%	20.0%	20.0%	12.0%	52.0%
M9	182.4	57.0	95.0	45.6	1308	555	177	0.466	48.0%	15.0%	25.0%	12.0%	52.0%
M10	182.4	95.0	57.0	45.6	1308	555	177	0.466	48.0%	25.0%	15.0%	12.0%	52.0%

3. Experimental Procedure

A performance-oriented experimental framework was adopted to establish multi-scale correlations between binder composition and structural behavior. Ten M30 concrete mixes were designed by systematically varying fly ash, GGBS, and Alccofine contents while maintaining constant total binder content and water–binder ratio. Compressive strength at 28 and 56 days was used for preliminary screening to capture hydration development and secondary reaction effects. On the basis of strength performance and variability, four mixes (M1, M2, M8, and M9) were shortlisted for further analysis. The shortlisted mixes were analyzed for compressive, split tensile, and flexural strength as per the standards. SEM-EDX analysis was carried out to investigate the

morphology of hydrates, pore structure, and elemental analysis. The reinforced concrete beams were subjected to two-point monotonic loading to assess the load-deflection characteristics, cracking pattern, stiffness loss, and failure behavior. Each reported value represents the mean of three specimens, and variability was quantified using standard deviation and coefficient of variation. The coefficient of variation for the measured properties ranged between 3% and 6%, indicating experimental consistency. The differences between the control mix and optimized mixes were analyzed using a two-tailed t-test at a confidence level of 95% to establish the significance of differences. One beam specimen was tested for each mix; therefore, the structural results should be interpreted as indicative rather than statistically representative.

3.1 Workability of Fresh Concrete

Workability test was done by slump test as per IS 1199:2018 [56]. The test was performed immediately after mixing using a standard slump cone apparatus. Concrete was placed in three layers, each compacted with 25 tamping strokes, followed by lifting the cone vertically to measure the slump.

3.2 Casting and Curing

Concrete specimens were cast and cured following a structured experimental framework to ensure systematic evaluation of mechanical properties and structural behavior. A total of ten mix proportions were initially developed for evaluation. Cube specimens were prepared and subjected to curing for 28 and 56 days to assess compressive strength and to identify the most suitable mix compositions based on strength performance. All specimens were water-cured at a temperature of 27 ± 2°C until the specified testing age. Based on strength-based screening, the selected mixes were subjected to further mechanical testing. After completion of the prescribed curing periods, reinforced concrete beam specimens were subsequently cast using the optimum mixes, cured for 28 days and tested to evaluate structural performance. The complete progression of casting and curing, specimen preparation and testing adopted in the study is expressed in Fig. 2.

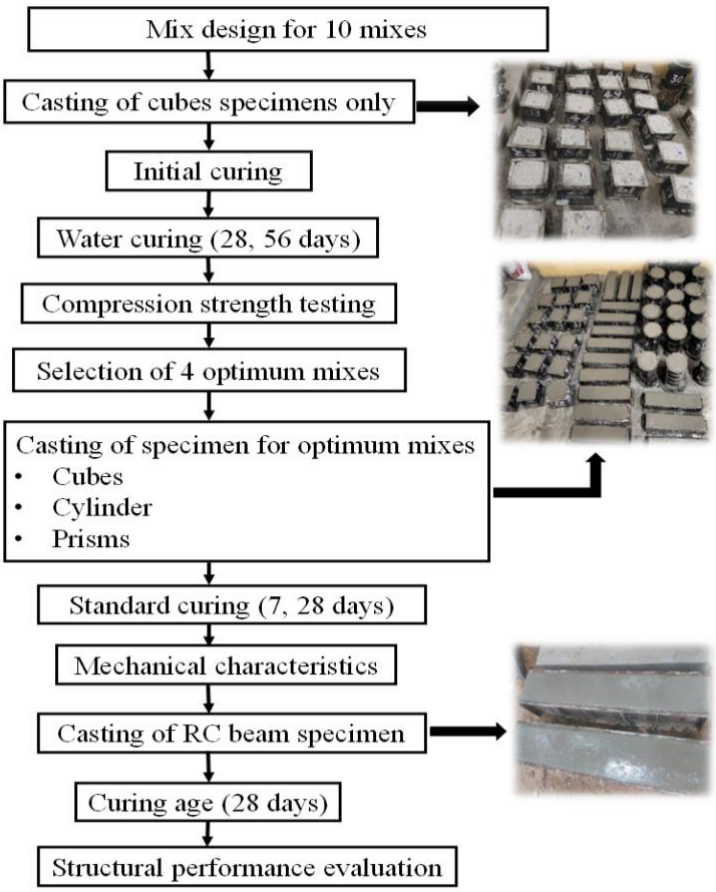

Fig. 2. Experimental workflow illustrating casting, curing, mechanical testing, and structural evaluation of concrete specimens and RC beams

3.3 Mechanical Properties

The mechanical properties of the concrete were determined in accordance with applicable Indian Standards. Compressive strength and flexural strength were measured on cubes and prisms specimens as per IS 516 [57]. Split tensile strength was determined on cylindrical specimens as per IS 5816 [58]. All specimens were properly cured prior to testing. For each test, three specimens were cast and tested and the average values were reported. The details of specimen types and counts are summarized in Table 4. Cube specimens of size 150 mm x 150 mm x 150 mm were used for compressive strength, cylindrical specimens of 150 mm x 300 mm were used for split tensile strength and prism specimens of 100 mm x 100 mm x 500 mm were used for flexural strength in accordance with relevant Indian standards.

Table 4. Summary of the specimen details

Specimen details	Count
Cubes	84
Cylinders	24
Prisms	24
Beams	4

3.4 Beam Design

The reinforced concrete beams in this study were designed in accordance with IS 456:2000 [57], with the objective of achieving a flexure-controlled failure. All beams were under-reinforced, ensuring that yielding of the tensile reinforcement preceded crushing of the concrete in the compression zone, which allows a clear assessment of the influence of supplementary cementitious materials (SCMs) on flexural behavior. Four concrete mixes were used: the control M1-PCC (plain cement concrete) and three SCM mixes incorporating fly ash (F), GGBS (G), and Alccofine (A)—M2 (F20–G20–A10), M8 (F20–G20–A12), and M9 (F15–G25–A12). All beams shared identical geometry (1500 mm x 230 mm x 230mm), reinforcement detailing, span, and support conditions, ensuring that variations in ultimate load and cracking behavior could be attributed solely to the SCM composition. Shear reinforcement was designed to be adequate in preventing shear failure, ensuring that all specimens failed by flexure. This design allows a direct assessment of the influence of various SCM combinations on the load-deflection behavior and cracking patterns of the reinforced concrete beam. The calculated flexural capacity (Mu) and shear capacity (Vu) for the critical section were 20.85 kN.m and 46.2 kN respectively, confirming that shear capacity significantly exceeded flexural demand, thereby ensuring flexural failure.

3.5 Beam Geometry and Reinforcement Details

The reinforced concrete beam specimens were compared with similar geometry and reinforcement details to provide a comparable structural response and thus facilitate the effect of concrete composition on flexural response. The beam had a square cross-section of 230 mm × 230 mm and a total length of 1500 mm, and was tested under simply supported conditions with an effective span of 1400 mm. A nominal clear concrete cover of 25 mm was provided as per IS 456:2000 [59]. The beams were designed as singly reinforced, under-reinforced flexural members to provide a flexural failure mode due to yielding of the tensile reinforcement before concrete crushing. Longitudinal tension reinforcement consisted of 12 mm diameter high-yield strength deformed bars, and nominal compression reinforcement was provided using 10 mm diameter bars. Adequate anchorage and development length were ensured as per IS-code provisions. To prevent premature shear failure and to ensure a flexure-controlled response, shear reinforcement was provided using 8 mm diameter closed stirrups at a uniform spacing of 130 mm c/c along the beam length. The shear reinforcement was designed such that the shear capacity exceeded the corresponding flexural demand, enabling stable crack development and reliable assessment of flexural

performance under monotonic loading. The geometry and reinforcement are illustrated in Fig. 3 and the detailing parameters are summarized in Table 5.

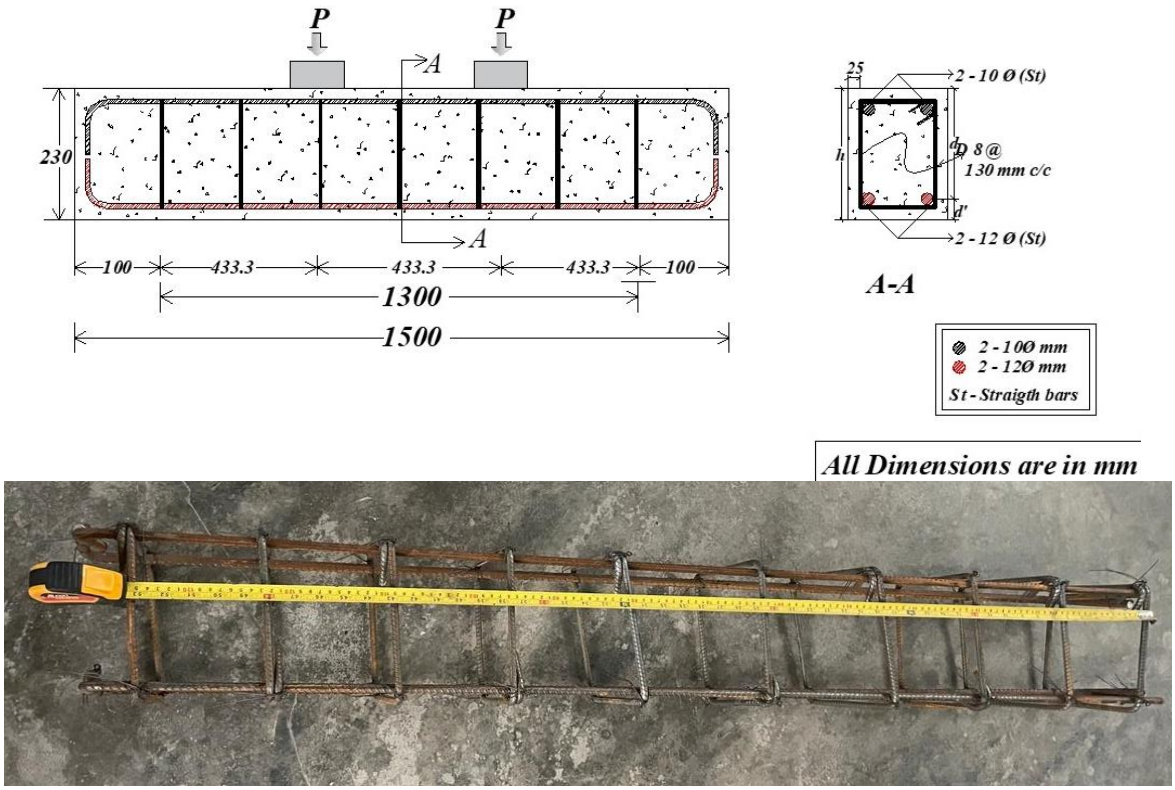

Fig. 3. Geometrical reinforcement details

Table 5. Reinforcement detailing parameters of RC beam specimens

b × D (mm)	L (mm)	Span (mm)	Cover (mm)	Tension steel	Compression steel	Stirrups	Steel grade	Support
230 × 230	1500	1400	25	2–12 mm	2–10 mm	8 mm @ 130 mm c/c	Fe 550	Simply supported

3.6 Test Setup and Instrumentation

All reinforced concrete beam specimens were tested under monotonic static loading. A simulated uniformly distributed load was applied through two symmetrically positioned concentrated point loads along the span. The beams were supported on a roller support at one end and a hinged support at the other providing a simply supported condition while allowing free rotation and minimizing restraint effects during testing. The applied load was delivered through a hydraulic loading frame provided with a calibrated load cell and transferred to the beam via a two-point loading arrangement, which effectively represents a uniformly distributed load over the central region of the span. This loading configuration was adopted to generate a constant bending moment region between the loading points thereby confirming that the beams were subjected predominantly to flexural action while limiting the influence of shear. Mid span deflection was measured using a linear variable differential transformer (LVDT) kept at the bottom of the beam. The LVDT was securely mounted to record the deflection during the test. The crack initiation and growth were also visually monitored and marked on the surface of the beam representing the flexural cracking pattern. The loading was incrementally applied until the occurrence of the first flexural cracks, and then it was continued until failure, which was indicated by a substantial loss of load-carrying capacity or excessive deflection. A schematic illustration of the test arrangement is

shown in Fig. 4. Crack width and crack spacing measurements were not instrumented and were assessed qualitatively; therefore, crack-related interpretations are based on visual observations.

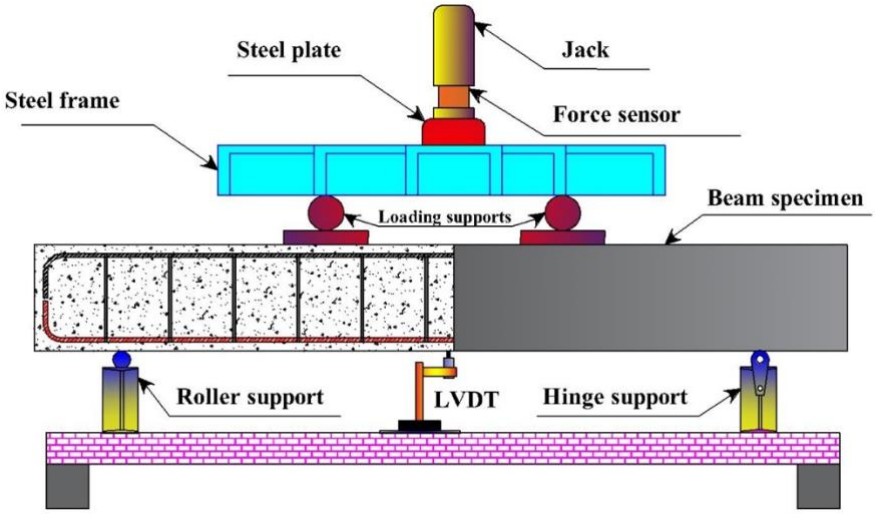

Fig. 4. Test setup and instrumentation

3.7 Microstructural Analysis

Microstructural analysis was conducted on the shortlisted optimal mixes to determine the direct correlation between the mechanical properties and the internal microstructural properties of the cementitious matrix. Scanning Electron Microscopy (SEM) and Energy Dispersive X-ray analysis (EDX) were used to investigate the hydration morphology, pore structure, and elemental composition. Representative particles were extracted from the interior of crushed concrete specimens after 28 days of compressive strength testing to ensure that the microstructural properties observed were representative of the hydration products and not altered by surface carbonation. SEM micrographs allowed the detailed observation of hydration products, matrix density, pore refinement, and interfacial transition zone (ITZ) quality. EDX spectra were utilized to provide phase identification using elemental composition and Ca-Si-Al maps to confirm the presence of C-S-H rich areas, ettringite-like morphology, and secondary aluminosilicate reaction products due to pozzolanic and latent hydraulic reactions. The combined SEM-EDX analysis provides supporting evidence for the observed mechanical performance, although it should not be interpreted as definitive proof of causation. Microstructural analysis demonstrates a denser cementitious matrix with diminished capillary porosity, a more consolidated interfacial transition zone and improved spatial distribution and interconnection of hydration products within the hardened composite. For each mix, multiple regions were examined, and representative micrographs were selected to ensure consistency of observations.

4. Results and Discussion

4.1 Workability

The variation in slump values across different mixes is presented in Fig. 5. An increase in workability is observed with the incorporation of supplementary cementitious materials. All mixes exhibited slump values within the acceptable range for reinforced concrete applications, indicating adequate workability suitable for proper placement and compaction of reinforced concrete without segregation. This behavior is attributed to improved particle packing and reduced internal friction within the concrete matrix.

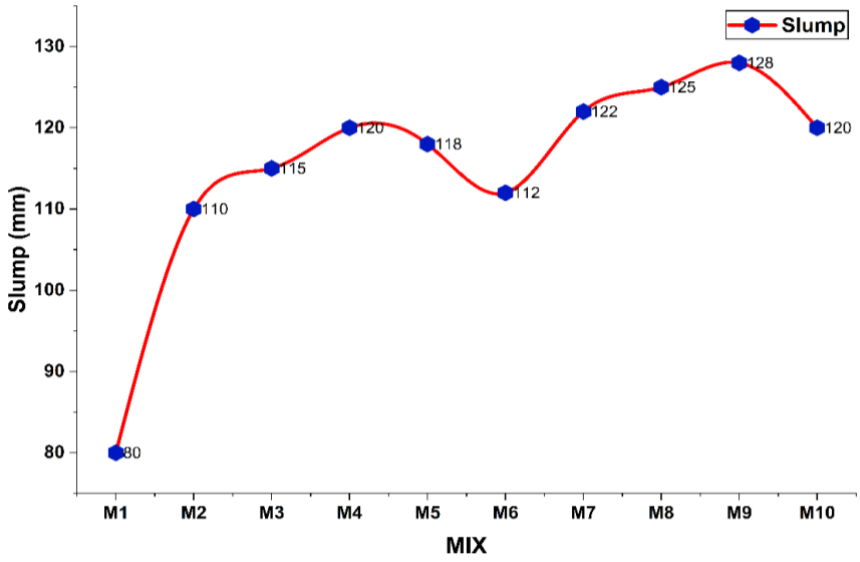

Fig. 5. The variation in slump values of different mixes

4.2 Compressive Strength

Minor variations in compressive strength between screening and detailed phases are due to separate casting batches at different experimental stages and do not affect the overall performance ranking. The compressive strengths recorded at 28 and 56 days (Table 6; Fig. 6(a)) vary from 24.87 to 47.12 MPa and from 29.6 to 52.1 MPa respectively. Error bars representing standard deviation are included in Fig. 6(a-d) to indicate variability in measured properties. The continued increase in strength from 28 to 56 days in the blended mixes reflects sustained hydration and persistent secondary reaction activity within the supplementary cementitious system. Based on this performance trend, mixes M1, M2, M8 and M9 were identified for detailed evaluation.

Table 6. Compressive strength of concrete mixes

MIX ID	Compressive strength (MPa)			
	Selection of optimum mix			
	28 days		56 days	
	Measured (MPa)	Enhancement (%)	Measured (MPa)	Enhancement (%)
M1	39.5	-	42.1	-
M2	43.69	10.60	45.2	7.40
M3	33.58	-15.0	39.5	-6.2
M4	32.05	-18.9	36.2	-14.0
M5	27.87	-29.4	31.7	-24.7
M6	33.94	-14.1	40.8	-3.1
M7	24.87	-37.0	29.6	-29.7
M8	46.14	16.80	50.3	19.50
M9	47.12	19.29	52.1	23.80
M10	40.93	3.60	44.3	5.20
	optimum mix			
	7 days		28 days	
	Measured (MPa)	Enhancement (%)	Measured (MPa)	Enhancement (%)
M1	23.0	-	39.5	-
M2	25.0	8.70	43.6	8.50
M8	26.4	14.80	46.14	14.80
M9	27.0	17.40	47.12	17.20

Their corresponding 7- and 28-day strength values are presented in Table 6 (optimum group) and Fig. 6(b), showing 28-day values of 39.5–47.12 MPa, exceeding the 30 MPa requirement for M30 grade concrete, thereby validating their suitability for subsequent tensile, flexural, stress–strain, microstructural, and beam-level studies. The compressive test setup is shown in Fig. 7(a). The improved performance observed in M8 and M9 indicates an effective interaction among the components of the ternary binder. Alccofine contributes to enhanced early-stage particle packing and accelerates nucleation of hydration products whereas fly ash and GGBS support continued reaction and progressive matrix densification at later ages. This complementary interaction supports continued strength development and enhances long-term retention.

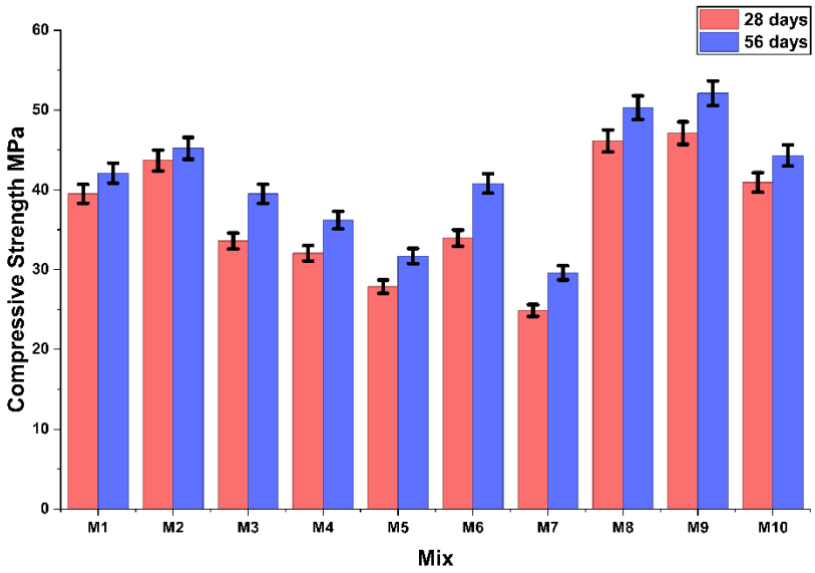

(a)

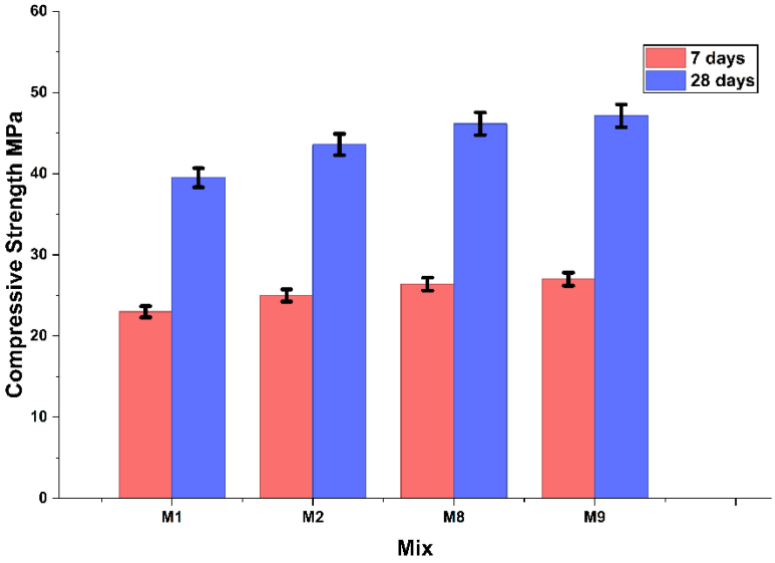

(b)

Fig. 6. (a). Compressive strength development of concrete mixes at 28 and 56 days and Fig. 6(b). Comparison of compressive strength of selected concrete mixes at 7 and 28 days

The superior performance of Mix M9 can be attributed to an optimal balance between calcium availability and reactive silica, which promotes the formation of a dense calcium–aluminosilicate hydrate gel network. Unlike higher replacement levels (e.g., M5 and M7), where excessive clinker dilution limits early hydration, M9 maintains sufficient calcium hydroxide for secondary reactions while enabling progressive microstructural densification. This balance enhances both early-age strength and long-term performance. Similar trends have been reported in recent studies on

ternary blended systems, where optimized combinations improve both packing density and hydration kinetics, leading to enhanced mechanical and structural response.

4.3 Split Tensile Strength

The split tensile strength results of the selected mixes at 7 and 28 days are illustrated in Table 7 and shown in Fig. 6(c). At 7 days, the tensile strength increased from 2.6 MPa for M1 to 3.6 MPa for M9. At 28 days, the corresponding values rose from 3.9 MPa (M1) to 5.2 MPa (M9). The experimental setup for the split tensile test is illustrated in Fig. 7(b). The tensile strength was found to increase with the curing age, signifying better resistance to crack formation and better stress transfer mechanisms in the cementitious matrix. This is related to the improved paste matrix continuity and ITZ refinement. The mechanical results are in line with the microstructural results presented in Section 6, which indicate lower pore connectivity and a denser ITZ in the ternary blended cements.

Table 7. Split tensile strength of concrete mixes at 7 and 28 days

MIX ID	Split Tensile Strength (MPa)			
	7 days		28 days	
	Measured (MPa)	Enhancement (%)	Measured (MPa)	Enhancement (%)
M1	2.6	-	3.9	-
M2	2.9	11.50	4.4	12.80
M8	3.3	26.90	4.9	25.60
M9	3.6	38.50	5.2	33.30

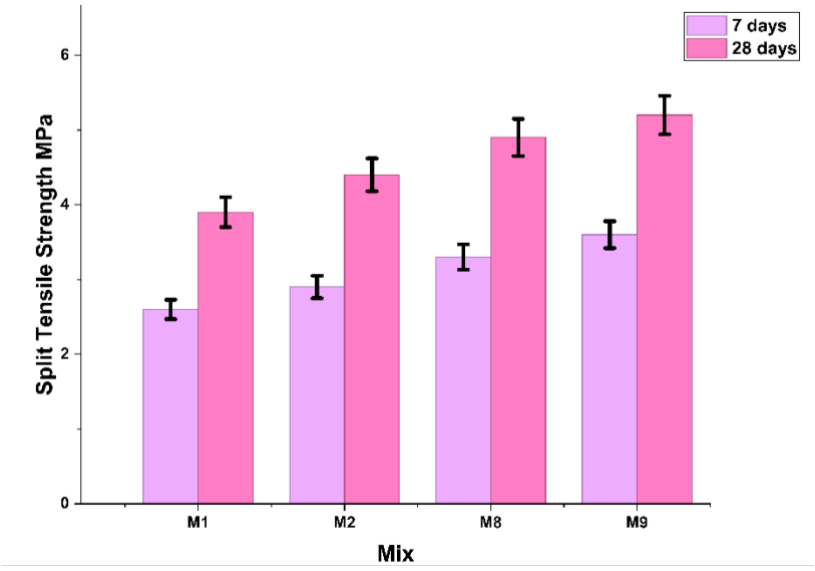

Fig. 6(c). Split tensile strength of selected concrete mixes at 7 and 28 days

4.4 Flexural Strength

The values of flexural strength at 7 and 28 days are given in Table 8 and Fig. 6(d). At 28 days, the flexural strength was found to increase from 6.5 MPa for M1 to 8.7 MPa for M9. The experimental setup for the flexural test is given in Fig. 7(c). The relatively larger increase in flexural strength compared to the compressive strength (Table 8 compared to Table 6) suggests that the ternary mixture is more effective in enhancing the tensile-dominated fracture properties. The increase in flexural strength is disproportionately higher than compressive strength, indicating improved tensile resistance and crack-bridging efficiency due to interfacial transition zone reinforcement. This can be attributed to the enhanced continuity of ITZs and the suppression of calcium hydroxide-rich regions, as evident from the SEM micrographs (Section 6)

Table 8. Flexural Strength of concrete mixes at 7 and 28 days

MIX ID	Flexural Strength (MPa)			
	7 days		28 days	
	Measured (MPa)	Enhancement (%)	Measured (MPa)	Enhancement (%)
M1	5.6	-	6.5	-
M2	6.2	10.71	7.4	13.85
M8	7.2	28.57	8.1	24.62
M9	7.4	32.14	8.7	33.85

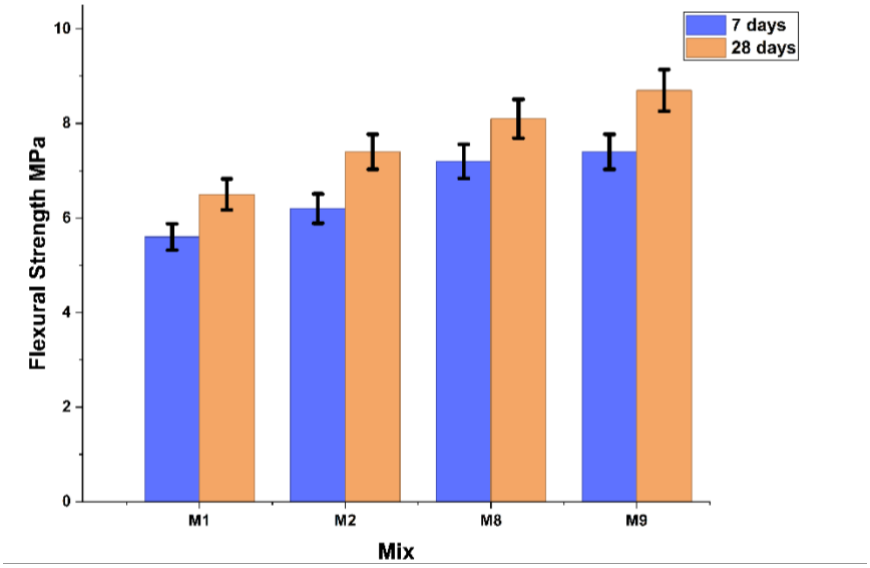

Fig. 6(d). Flexural strength of selected concrete mixes at 7 and 28 days

(a) (b) (c)

Fig. 7. Experimental setup (a) compression strength test, (b) split tensile test & (c) flexural strength test

5. Structural Performance

The flexural performance of the reinforced concrete beams indicated an improvement in structural behavior following the optimization of ternary blended binder compositions. Compared to the control beam, the specimens containing fly ash–GGBS–Alccofine blends exhibited higher ultimate load capacity, improved curvature ductility, and enhanced post-cracking stiffness retention. The smoother transition from linear elastic to nonlinear behavior, along with moderated stiffness degradation, is consistent with a more distributed cracking mechanism and improved internal stress transfer. These results indicate that the refinement of binder composition at the material level is reflected in the structural performance at the member level. For the clarity of presentation, the reinforced concrete control beam is referred to as RC-CB-1 (M1), where RC-CB stands for

reinforced concrete control beam, whereas the ternary blended beams are referred to as RC-TB-2 (M2), RC-TB-3 (M8), and RC-TB-4 (M9), where RC-TB stands for reinforced concrete ternary beam.

5.1 Load–Deflection Behavior of Beams

The load-deflection curves for all beams under monotonic two-point loading are shown in Fig. 8. These curves illustrate the typical under-reinforced behavior, which consists of an initial linear and elastic portion, followed by a stiffness degradation after cracking, nonlinear deformation evolution, and finally post-peak softening. The control beam (M1) attained an ultimate load of 112.00 kN, as seen in Fig. 8(a). The ternary beams showed an increasingly higher ultimate load resistance, with M2, M8, and M9 reaching 116.26 kN, 120.00 kN, and 124.60 kN, respectively (Fig. 8(b-d)). The optimized mix proportion (M9) showed an 11.3% increase in ultimate load resistance over the OPC control. Following the peak load, the control beam experienced a sudden loss of load-carrying capacity, characteristic of localized crushing in the compression zone. Compared to the control, the ternary blended beams exhibited a less sudden post-peak stiffness degradation, which is consistent with a more distributed cracking mechanism and improved internal stress transfer which can be attributed to the improved microstructural uniformity and refined interfacial transition zone that facilitate more distributed cracking and gradual stress transfer within the concrete matrix.

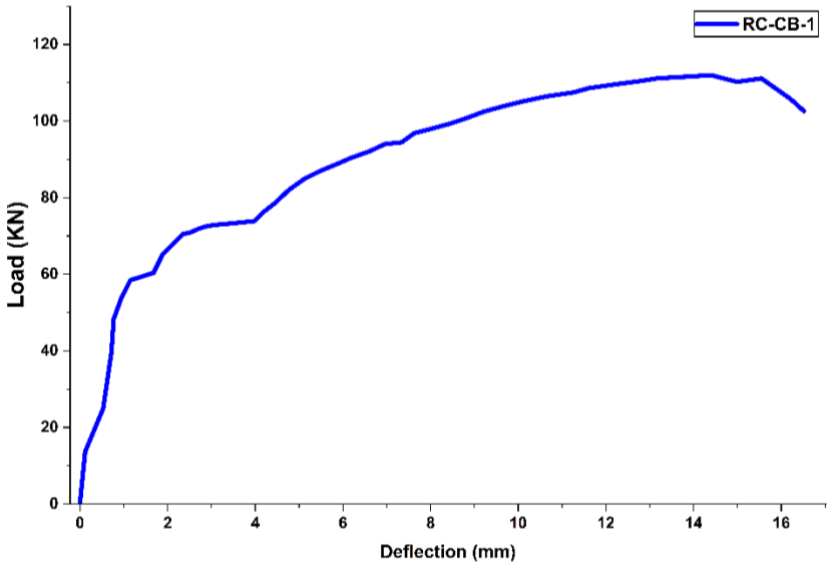

(a)

Fig. 8

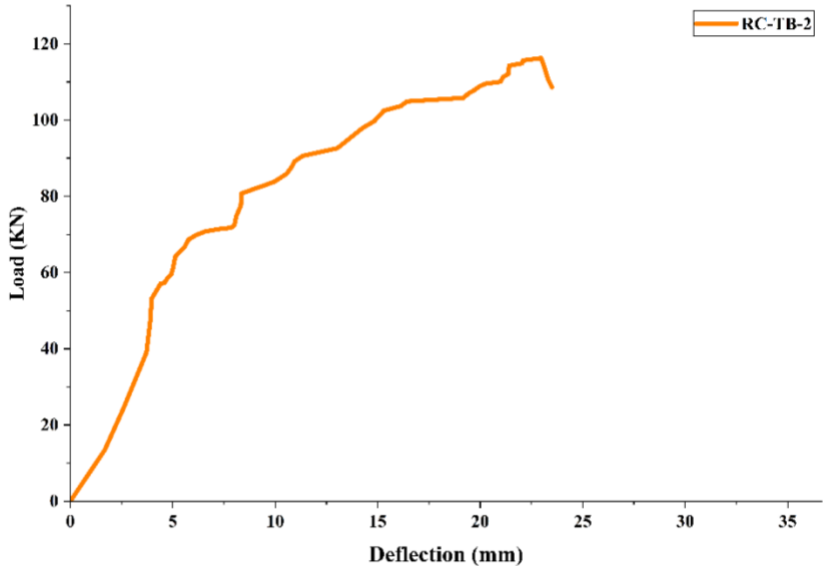

(b)

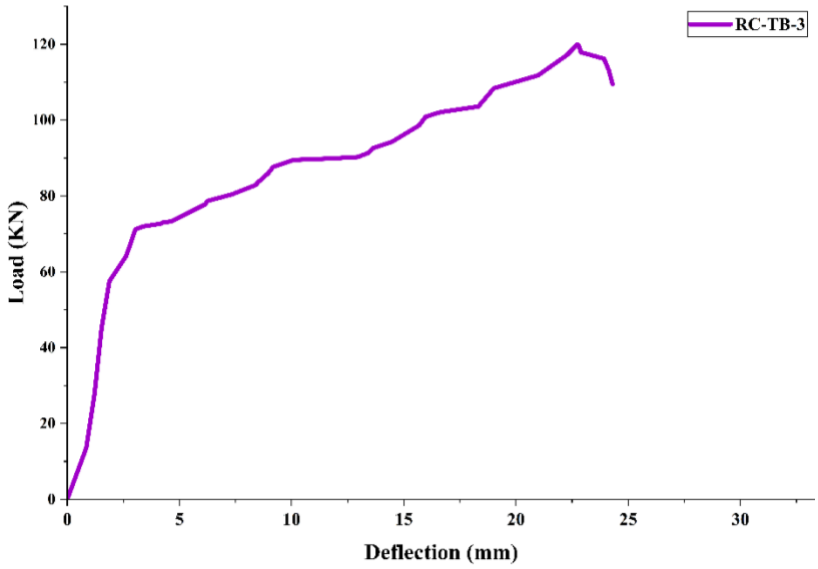

(c)

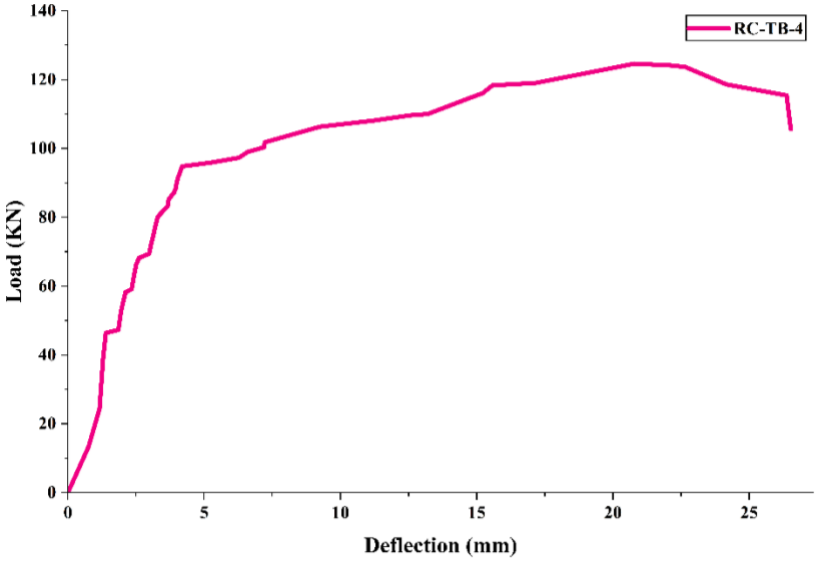

(d)

Fig. 8. Load–deflection response of control beam (a) RC-CB-1, (b) RC-TB-2, (c) RC-TB-3, and (d)RC-TB-4

5.2 Experimental ss Theoretical Flexural Capacity

The comparison between the predicted and actual moment capacities is given in Table 9. The ultimate flexural strength was calculated on the basis of strain compatibility for a doubly reinforced rectangular section, as per IS 456:2000. The cross-section of the beam was 230mm × 230 mm with an effective depth of 180 mm, area of tension reinforcement 191.63 mm^2, area of compression reinforcement 157.08 mm^2 (2-10 mm bars), and strength of steel 550 MPa. The shear span was 0.433 m

Table 9. Experimental and theoretical flexural moment capacity of RC beams

Beam	$M_{u,th}$	$M_{u,exp}$	$M_{u,exp}/ M_{u,th}$
M1	19.82	24.25	1.22
M2	20.36	25.17	1.24
M8	20.71	25.98	1.25
M9	20.85	26.98	1.29

Experimental capacities exceeded theoretical predictions by 22–29%, reflecting conservative stress-block assumptions, compression steel contribution, and tension stiffening effects. The

progressive increase in moment capacity tends to confirm that binder refinement improves the efficiency of the compression zone with no negative effect on under-reinforced bending.

5.3 Crack Pattern and Failure Characteristics

Typical crack patterns at ultimate load are presented in Fig. 9(a–d). In all beams, flexural cracks originated in the constant moment zone and then propagated vertically towards the compression zone. The control beam (Fig. 9a) had fewer but wider cracks, reflecting an earlier stage of crack localization and lower tension stiffening. In contrast, beams M2 and M8 (Fig. 9b–c) exhibited a greater number of finer, more uniformly distributed cracks, suggesting improved bond behavior and strain compatibility between concrete and reinforcement, likely due to the densification of the interfacial transition zone and reduced micro-porosity, which enhances stress transfer across the steel–concrete interface. The optimized beam M9 (Fig. 9d) demonstrated the most refined crack distribution with delayed crack widening and improved spatial spread. This behavior is consistent with enhanced interfacial transition zone densification observed in SEM analysis. All specimens ultimately failed in a flexure-dominated mode characterized by yielding of tensile reinforcement followed by compression zone crushing, confirming under-reinforced behavior consistent with strain compatibility assumptions.

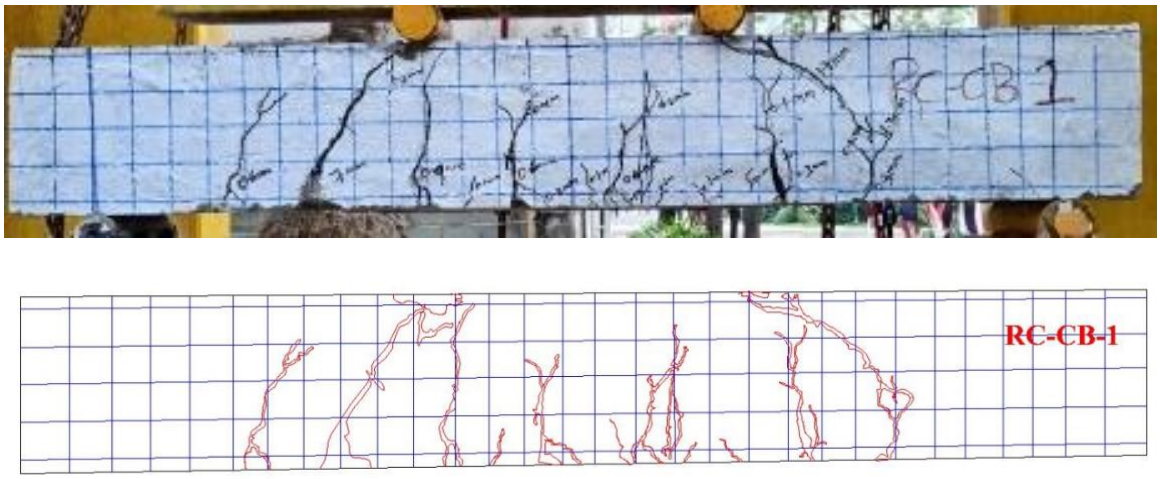

(a)

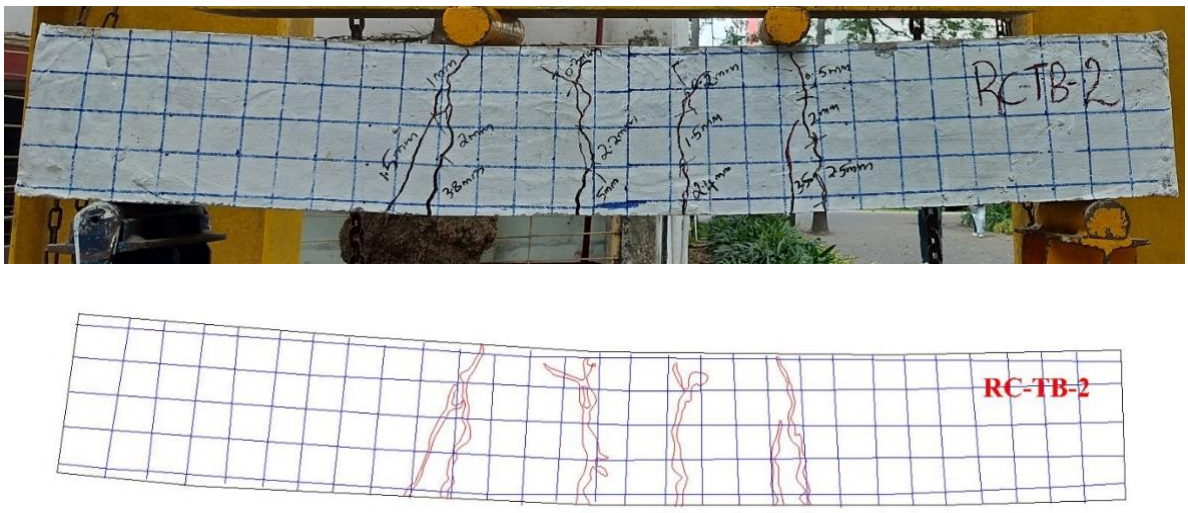

(b)

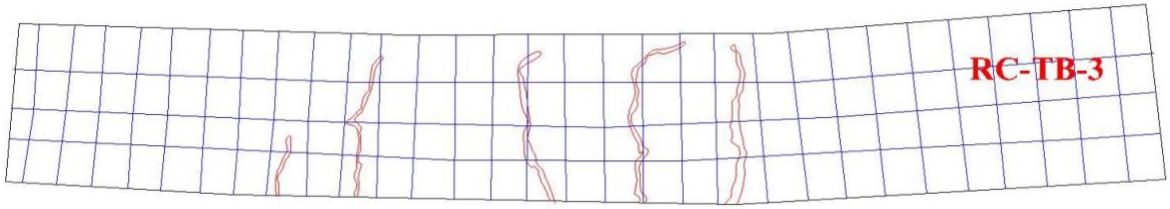

(c)

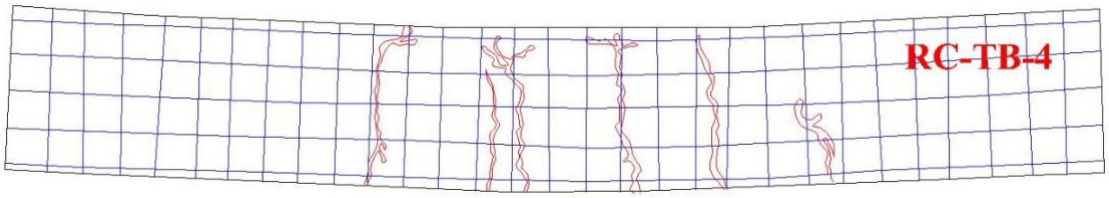

(d)

Fig. 9. Crack pattern and failure characteristics of beam specimens (a) RC-CB-1, (b) RC-TB-2, (c) RC-TB-3 & (d) RC-TB-4

5.4 Ductility and Stiffness Degradation

The deformation capacity of the reinforced concrete beams was quantified using a deflection-based ductility index derived from the load–deflection responses shown in Fig. 8. The ductility index was computed as $\mu=\Delta u/\Delta y$, where Δy is the mid-span deflection corresponding to 0.75Pu on the ascending branch of the load–deflection curve and Δu is the ultimate mid-span deflection at failure. The evaluated parameters are presented in Table 10.

Table 10. Ductility parameters obtained from load- deflection response

Beam (Mix)	Pu (kN)	Δu (mm)	Δy at 0.75Pu (mm)	μ = Δu/Δy
M1	112.00	16.52	7.50	2.20
M2	116.26	23.50	8.90	2.64
M8	120.00	24.30	9.10	2.67
M9	124.60	26.50	9.80	2.70

The ductility index increased from 2.20 in the control beam (M1) to 2.70 in the optimized beam (M9) while the ultimate deflection increased by 60% relative to the control. The control specimen showed a marked loss of stiffness after cracking, indicative of localized damage development and early compression-zone softening. Conversely, the ternary blended beams experienced greater deformations with a softer slope of the secant stiffness and a shallower slope in the post-peak

region. The cracking pattern distribution shown in Fig. 9, and the softer slope of the descending part in Fig. 8, further verifies the above-mentioned phenomenon. The experimental results indicate that ternary binder refinement improves deformation capacity while maintaining the same under-reinforcement failure mode.

6. Microstructural Characteristics

The SEM micrographs of the control mix (Fig. 10(a–c)) reveal a heterogeneous cementitious matrix with a predominance of primary hydration products. Regions exhibiting morphology consistent with C–S–H phases were observed; however, phase identification based on visual characteristics remains indicative rather than definitive. The interfacial transition zone (ITZ) is relatively porous, with a discontinuous gel region and CH concentration. The microstructural inhomogeneities cause localized stiffness changes and provide easy paths for the development of cracks under tensile loading. The presence of partially hydrated cement particles, along with pore networks, indicates poor packing density and an underdeveloped hydration gel structure. The microstructural characteristics are in line with the lower tensile strength and the relatively brittle post-peak response of the control specimen. This study establishes a direct correlation between ternary binder composition, microstructural refinement and flexural behavior at the structural level, which remains insufficiently addressed in existing literature.

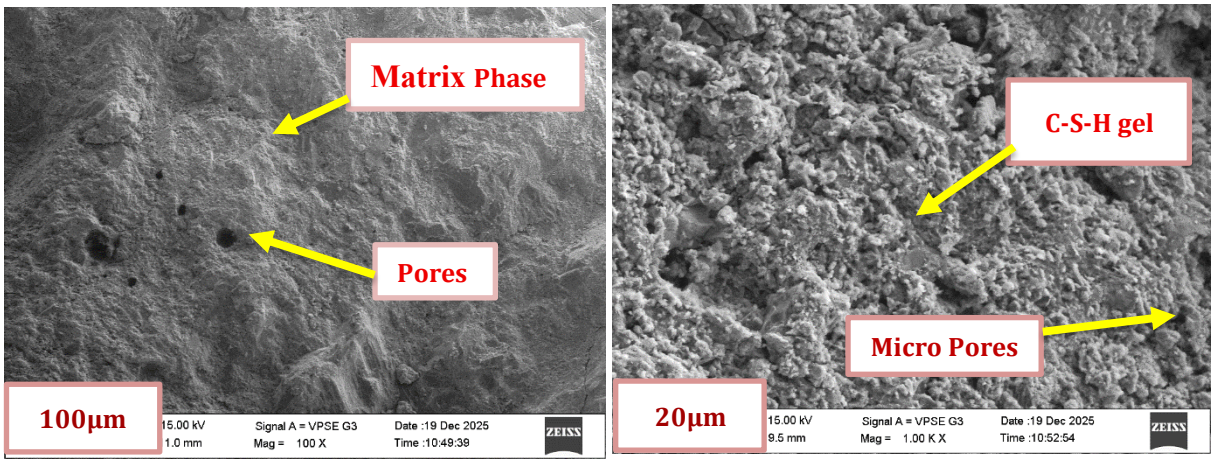

(a) (b)

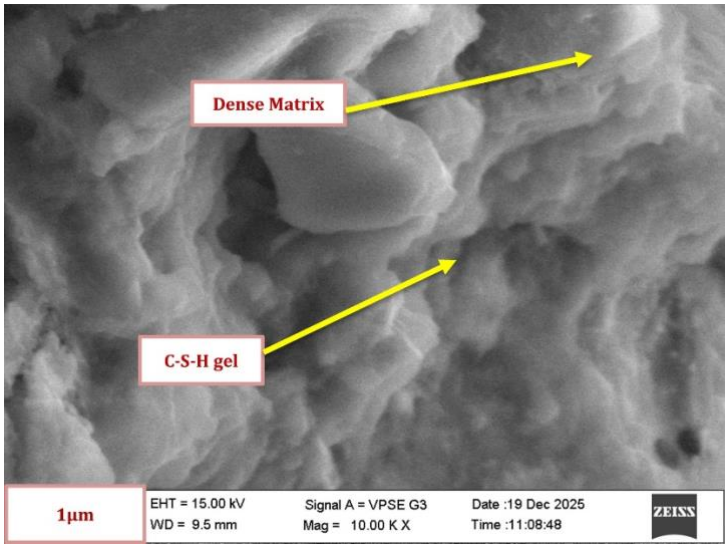

(c)

Fig. 10. SEM micrographs of control mix M1 at (a) low (b) medium & (c) high magnification.

6.1 Microstructural Characteristics of Mix M2

SEM micrographs of Mix M2 (Fig. 11a–c) reveal a denser and more uniform matrix compared to the control. A marked reduction in the size and number of calcium hydroxide (CH) crystals indicates the presence of pozzolanic activity. The hydration products are more continuous, signifying better phase integration. The interfacial transition zone (ITZ) is relatively denser, with reduced pore connectivity and better bonding between the matrix and aggregates.

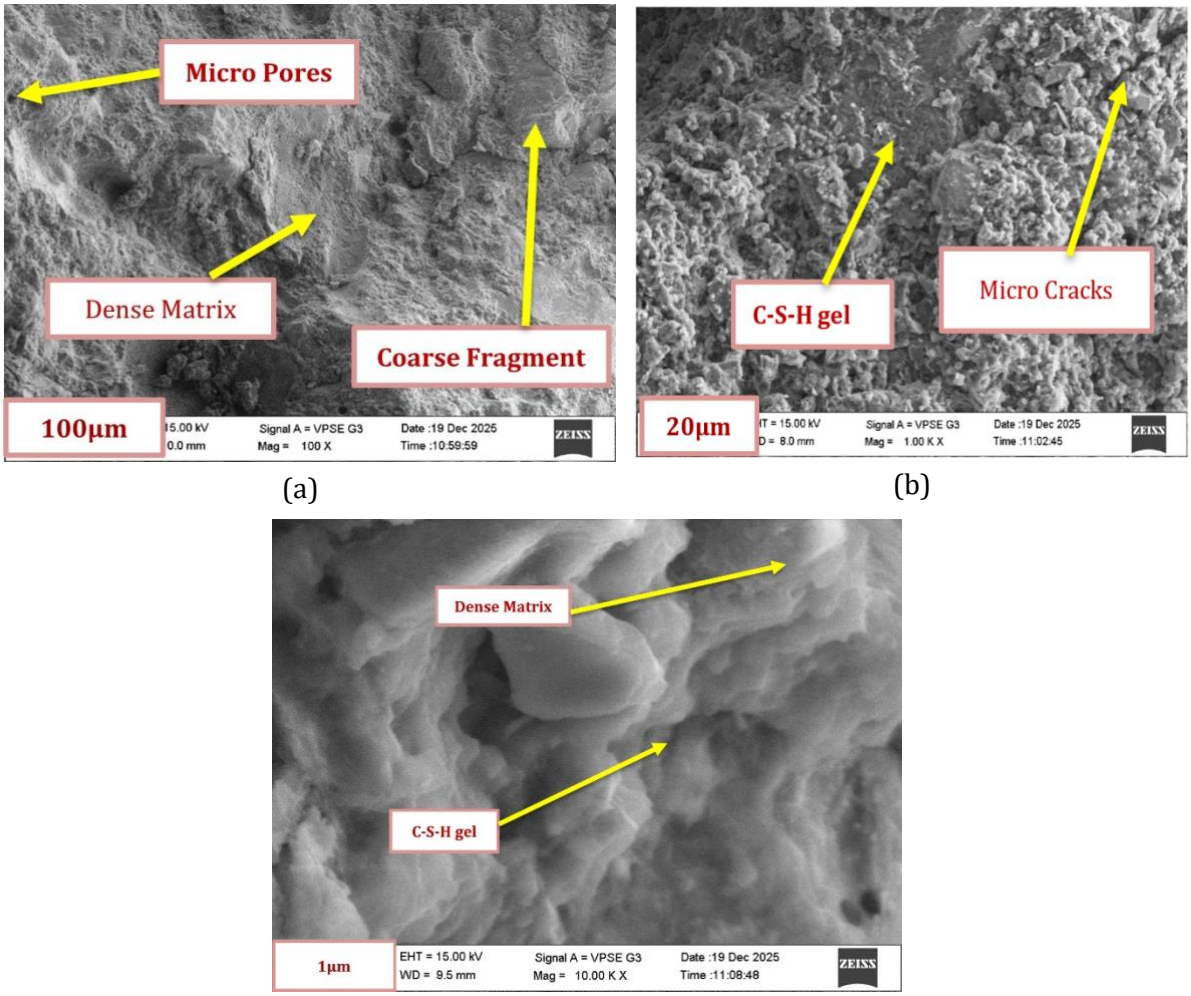

Fig. 11. SEM micrographs of mix M2 at (a) low (b) medium & (c) high magnification.

6.1.1 Microstructural Characteristics – Mix M8

Mix M8 (Fig. 12a–c) shows significant pore refinement and a reduced incidence of microcracks. The matrix looks dense with fewer portlandite deposits, signifying a good interaction between fly ash, GGBS, and Alccofine. The improved spatial continuity of the hydration phases increases the efficiency of load transfer in the cementitious matrix

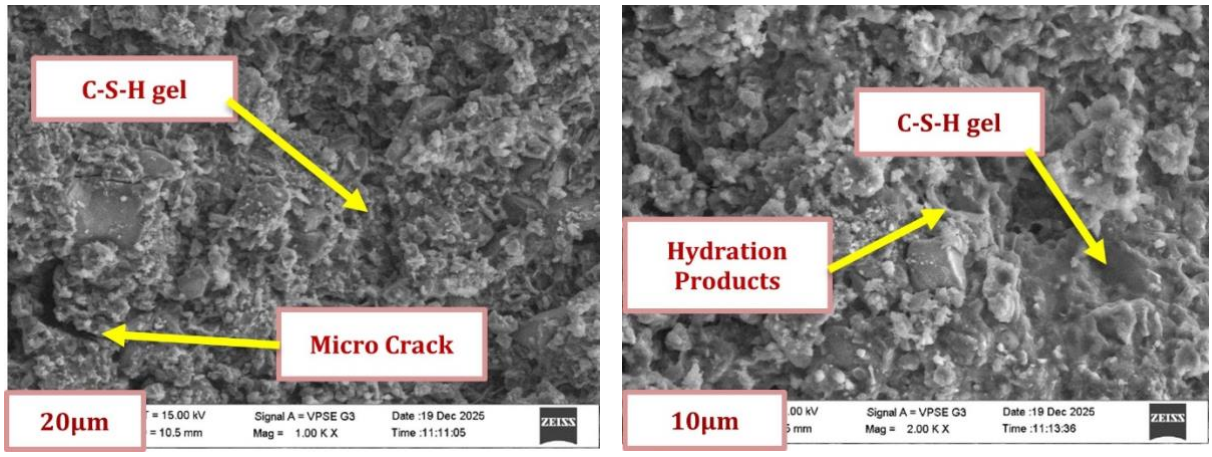

(a) (b)

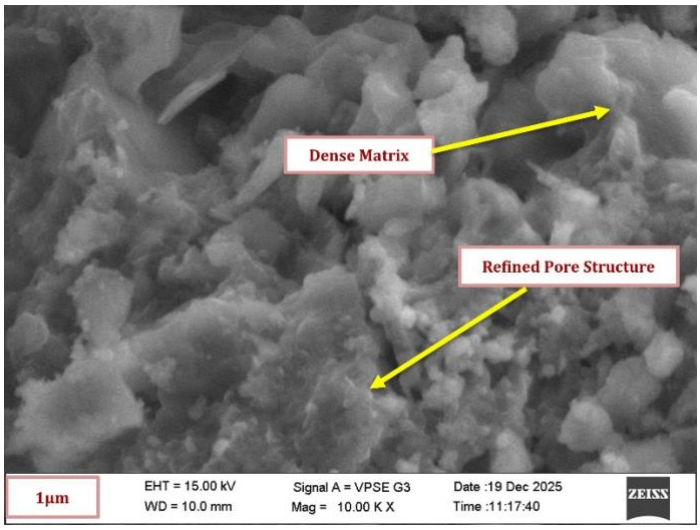

(c)

Fig. 12. SEM micrographs of mix M8 at (a) low (b) medium and (c) high magnification

6.1.2 Microstructural Characteristics – Mix M9

Mix M9 (Fig. 13a–c) has the most advanced microstructure. Features indicative of C-A-S-H-type phases and reduced capillary porosity are observed. The ITZ zone is very dense and continuous, which is conducive to enhanced tensile strength and resistance to crack localization.

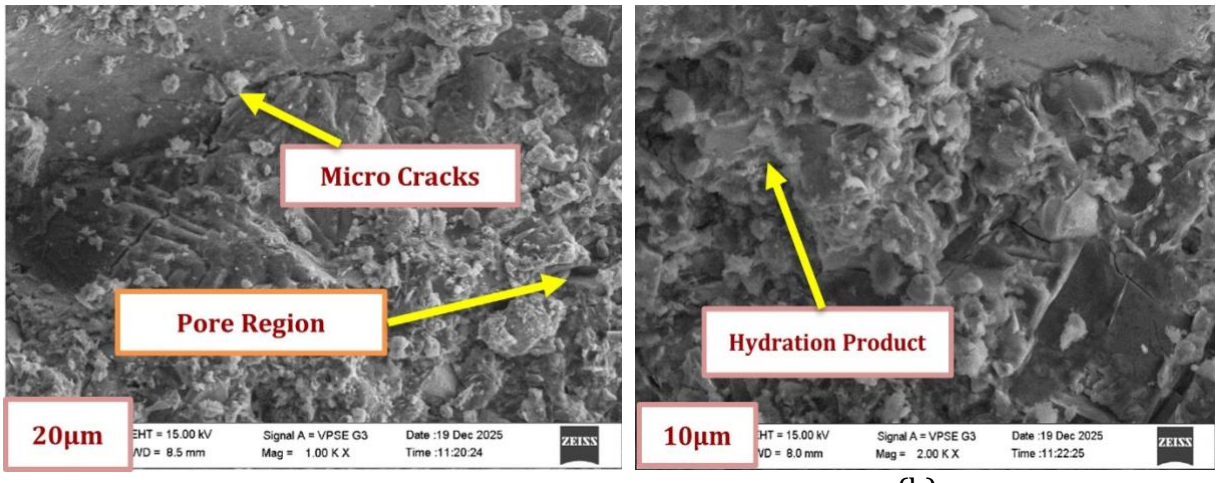

(a) (b)

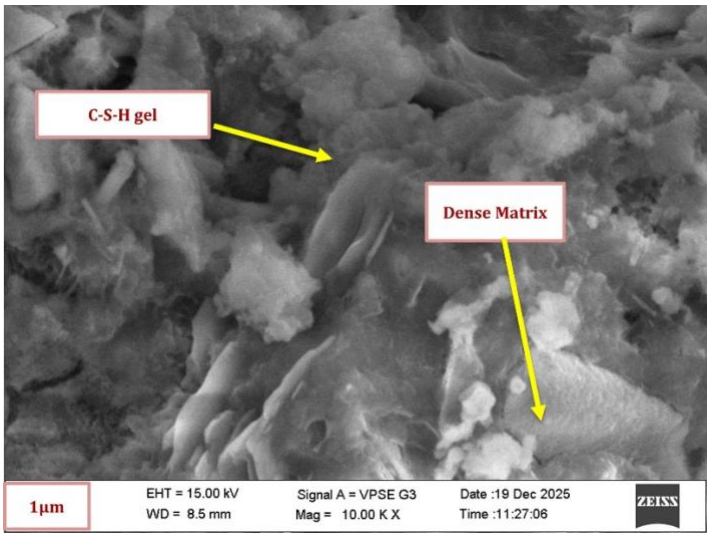

(c)

Fig. 13. SEM micrographs of mix M9 at (a) low (b) medium & (c) high magnification.

The gradual increase in microstructural density from M1 to M9 clearly indicates that ternary synergy promotes microstructural stability. It should be noted that SEM observations are primarily morphological in nature and therefore identification of hydration phases is based on visual features rather than definitive phase confirmation. Consequently, microstructural interpretations are presented as supportive evidence and should be considered in conjunction with mechanical and structural results.

7. EDX Analysis

The EDX spectra of Mixes M1, M2, M8, and M9 are given in Fig. 14–17, and the corresponding atomic percentages are given in Table 11. The control mix (M1) has a Ca/Si ratio of 4.86, indicating a calcium-rich matrix due to the presence of portlandite. The addition of supplementary cementitious materials causes a drastic decrease in the Ca/Si ratio. Mix M2 shows the lowest ratio of 1.41, while Mix M8 shows an intermediate ratio of 2.60. The efficient mix M9 has a Ca/Si ratio of 1.76, indicating a significant consumption of calcium hydroxide consumption and better silicate incorporation into the hydrate matrix. Although Mix M2 shows the lowest Ca/Si ratio, Mix M9 achieves better mechanical and structural properties. This indicates that the enhancement of strength is not dependent on the Ca/Si ratio but on the combined influence of hydrate chemistry modification, ultrafine particle packing, pore refinement, and ITZ modification. While Ca/Si ratio provides useful insight into hydration chemistry, it cannot independently explain mechanical performance and is therefore used only as a supportive indicator.

Table 11. Elemental composition and Ca/ Si atomic ratio of concrete mixes obtained from EDX analysis

MIX ID	C%	O%	Mg%	Al%	Si%	K%	Ca%	Fe%	Ca/Si
M1	0.4	64.1	0.6	1.4	5.2	0.8	25.3	1.5	4.86
M2	0.2	73.2	1.9	3.6	8.0	0.9	11.3	0.9	1.41
M8	0.1	66.6	1.1	2.6	7.5	1.0	19.5	1.6	2.60
M9	6.9	64.6	1.4	3.5	8.2	-	14.4	1.0	1.76

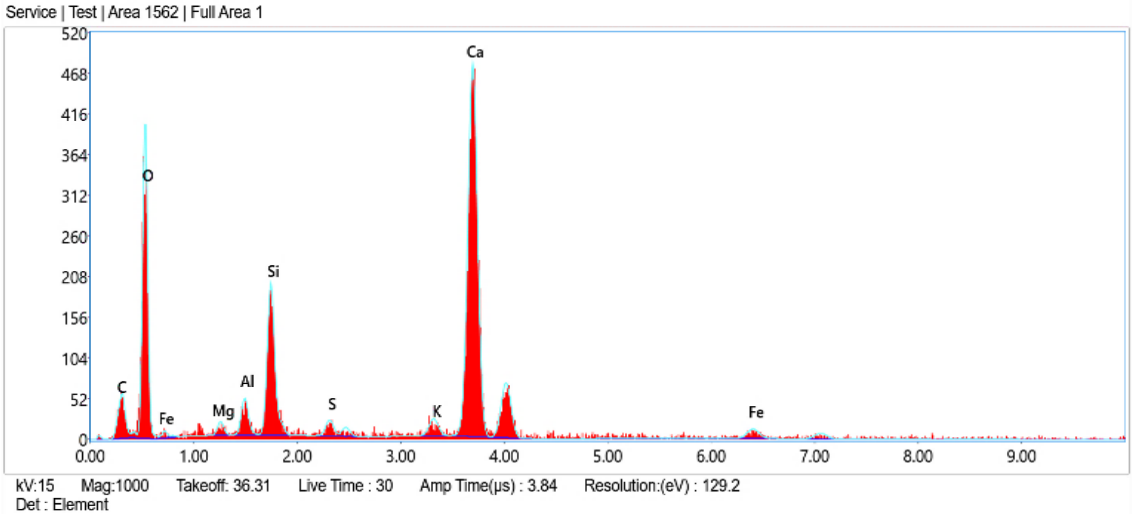

Fig. 14. EDX Analysis of Mix 1

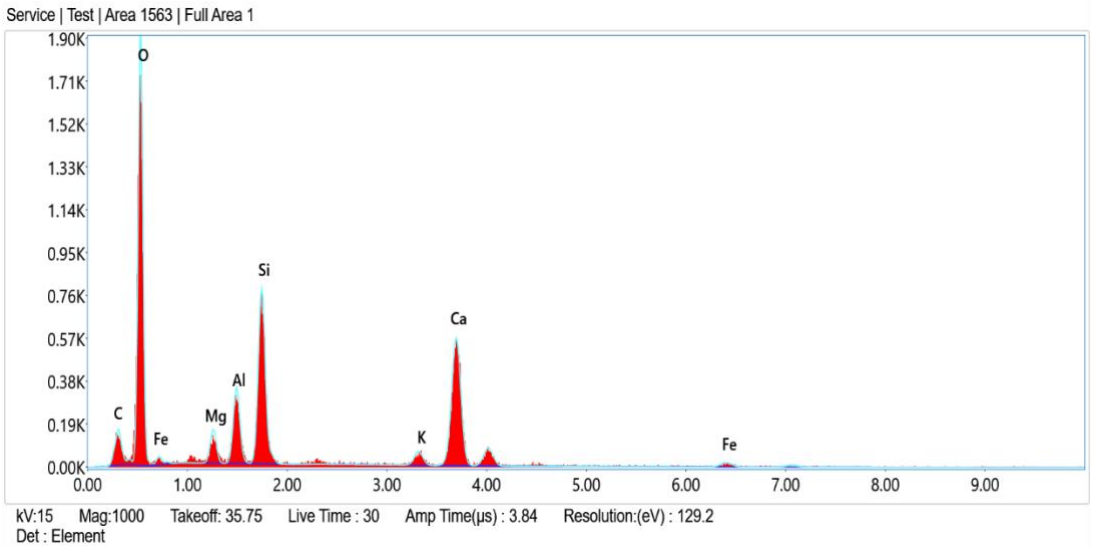

Fig. 15. EDX Analysis of Mix 2

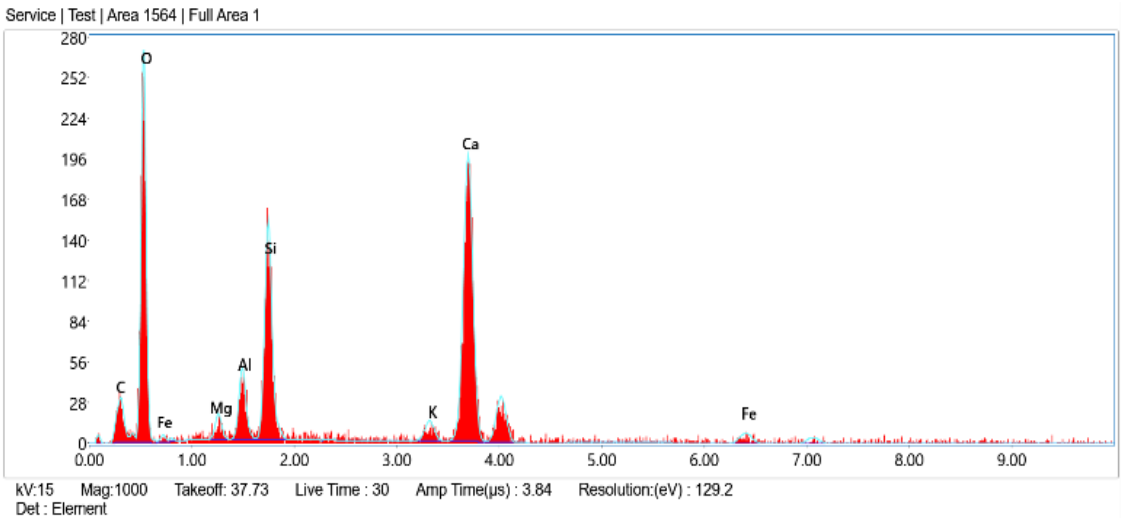

Fig. 16. EDX Analysis of Mix 8

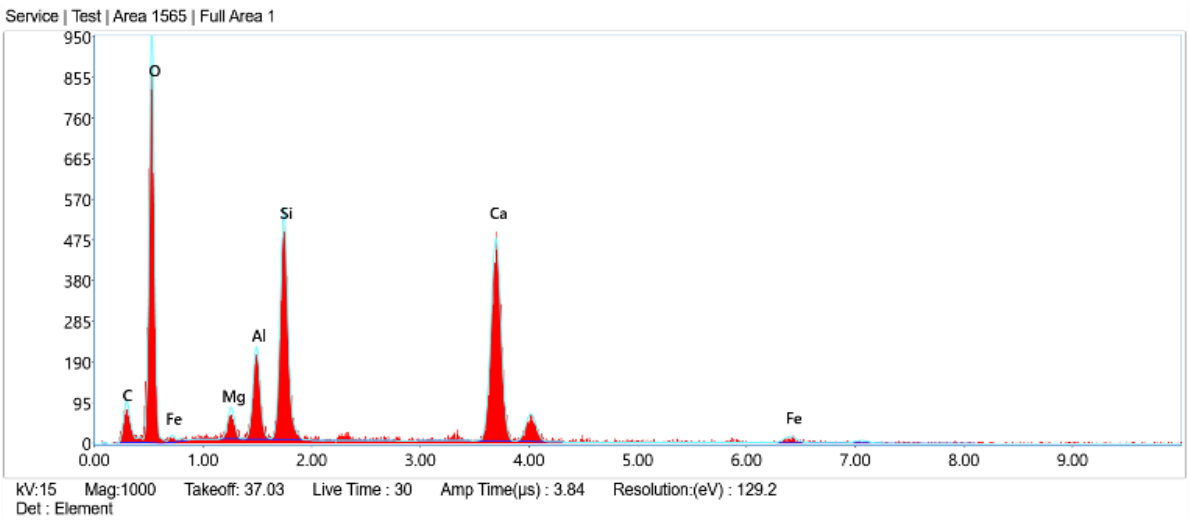

Fig. 17. EDX Analysis of Mix 9

8. Sustainability Implications

The optimized proportion (M9) resulted in 52% clinker substitution compared to the reference concrete. The cement content reduced from 380 kg/m^3 to 182.4 kg/m^3, which in turn led to a reduction of 197.6 kg of cement per cubic meter of concrete. Based on an emission factor of 0.9 kg CO_2 per kg of cement, this translates to a reduction of 178 kg CO_2 per cubic meter of concrete. This calculation takes into account the cement phase emissions alone and does not account for embodied emissions of supplementary cementitious materials or transportation. Although there is a reduction in the amount of clinker, the optimized proportion has a higher load-carrying capacity and deformation behavior at a structural scale, which in turn indicates better carbon efficiency per unit structural performance. The findings validate that a substantial amount of clinker can be reduced without affecting the mechanical performance or member-level behavior. When compared to the embodied carbon reduction, the optimized proportion has better structural carbon efficiency, as it has a higher load-carrying capacity per unit CO_2 emission than the OPC reference. The analysis considers only cement-phase emissions and does not account for full life-cycle impacts, and therefore conclusions are limited to relative clinker reduction benefits.

9. Conclusion

This study presents a comprehensive experimental investigation into the mechanical, structural, and microstructural performance of ternary blended concrete incorporating fly ash, ground granulated blast furnace slag, and Alccofine. By adopting a multi-scale approach, the study establishes a direct correlation between binder composition, hydration characteristics, and the flexural behavior of reinforced concrete members, thereby attempting to address a critical gap in existing literature that predominantly focuses on material-level properties.

The experimental results demonstrate that the optimized mix (M9) achieves a well-balanced enhancement in performance across multiple scales. At the material level, compressive strength improved by 19.29%, while more significant gains were observed in tensile-dominated properties, with split tensile and flexural strengths increasing by 33.3% and 33.85%, respectively. These results indicate that ternary binder systems are particularly effective in enhancing crack resistance and tensile load transfer mechanisms, which are critical for structural applications.

At the structural level, reinforced concrete beams exhibited an increase of approximately 11.3% in ultimate load-carrying capacity, along with improved deformation capacity and ductility. The load–deflection response showed a smoother transition from elastic to nonlinear behavior, reduced stiffness degradation, and enhanced post-cracking response. The observed crack patterns, characterized by a greater number of finer and more uniformly distributed cracks, suggest improved bond characteristics and more effective stress redistribution within the concrete matrix.

Microstructural analysis revealed a denser cementitious matrix with reduced pore connectivity and a refined interfacial transition zone, supporting the observed improvements in mechanical and structural performance. However, these observations are interpreted as supportive rather than conclusive, and the enhanced behavior is attributed to the combined effects of particle packing, secondary hydration reactions, and progressive microstructural densification.

In addition to performance improvements, the optimized mix achieved approximately 52% clinker substitution, resulting in a substantial reduction in cement consumption and associated carbon emissions. While this indicates significant potential for sustainable construction, environmental assessment is limited to cement-phase emissions and does not represent a complete life-cycle analysis. Overall, the findings demonstrate that ternary blended systems can effectively enhance structural performance while contributing to sustainability objectives, providing a viable pathway for the development of high-performance, low-carbon concrete.

9.1 Future Scope

Although the current study has proven the structural feasibility of optimized ternary binder systems on a beam scale, further research is needed to evaluate their long-term performance characteristics in actual service conditions. Future studies should be aimed at investigating their durability performance in aggressive environments, time-dependent behavior including creep and shrinkage, and validation at a larger structural scale. Incorporation of experimental data into nonlinear analytical models would be helpful in this regard. Furthermore, life-cycle assessment studies encompassing transportation, processing, and service life aspects are also recommended to estimate the comprehensive environmental impact of these systems

References

[1] Scrivener KL, John VM, Gartner EM. Eco-efficient cements: Potential economically viable solutions for a low-CO2 cement-based materials industry. Cem Concr Res. 2018 Dec;114:2-26. https://doi.org/10.1016/j.cemconres.2018.03.015

[2] Knight KA, Cunningham PR, Miller SA. Optimizing supplementary cementitious material replacement to minimize the environmental impacts of concrete. Cem Concr Compos. 2023 May;139:105049. https://doi.org/10.1016/j.cemconcomp.2023.105049

[3] Prakasan S, Palaniappan S, Gettu R. Study of Energy Use and CO2 Emissions in the Manufacturing of Clinker and Cement. J Inst Eng (India): Series A. 2020 Mar;101(1):221-32. https://doi.org/10.1007/s40030-019-00409-4

[4] Antunes M, Santos RL, Pereira J, Rocha P, Horta RB, Colaço R. Alternative clinker technologies for reducing carbon emissions in cement industry: A critical review. Materials. 2022 Jan 1;15(1):209. https://doi.org/10.3390/ma15010209

[5] Andrew RM. Global CO2 emissions from cement production, 1928-2018. Earth Syst Sci Data. 2019 Nov;11(4):1675-1710. https://doi.org/10.5194/essd-11-1675-2019

[6] Andrew RM. A comprehensive analysis of process-related CO2 emissions from Iran's cement industry. Clean Environ Syst. 2025 Mar;16:100251. https://doi.org/10.1016/j.cesys.2024.100251

[7] Khaiyum MZ, Sarker S, Kabir G. Evaluation of Carbon Emission Factors in the Cement Industry: An Emerging Economy Context. Sustainability. 2023 Nov;15(21):15407. https://doi.org/10.3390/su152115407

[8] Volaity SS, et al. Towards decarbonization of cement industry: a critical review of electrification technologies for sustainable cement production. npj Mater Sustain. 2025 Jul;3(1):68. https://doi.org/10.1038/s44296-025-00068-6

[9] Bacharz M, Bacharz K, Trąmpczyński W. Impact of Early-Age Curing and Environmental Conditions on Shrinkage and Microcracking in Concrete. Materials. 2025 Jul;18(13):3185. https://doi.org/10.3390/ma18133185

[10] Neville AM. Properties of Concrete. 5th ed. Prentice Hall; 2012.

[11] Zhou Y, Gencturk B, Willam K, Attar A. Carbonation-Induced and Chloride-Induced Corrosion in Reinforced Concrete Structures. J Mater Civ Eng. 2015 Sep;27(9):0001209. https://doi.org/10.1061/(ASCE)MT.1943-5533.0001209

[12] Skibsted J, Snellings R. Reactivity of supplementary cementitious materials (SCMs) in cement blends. Cem Concr Res. 2019 Oct;124:105799. https://doi.org/10.1016/j.cemconres.2019.105799

[13] Franco de Carvalho JM, de Melo TV, Fontes WC, dos Santos Batista JO, Brigolini GJ, Peixoto RAF. More eco-efficient concrete: An approach on optimization in the production and use of waste-based

supplementary cementing materials. Constr Build Mater. 2019 May;206:397-409. https://doi.org/10.1016/j.conbuildmat.2019.02.054
[14] Fuzail Hashmi A, Shariq M, Baqi A, Haq M. Optimization of fly ash concrete mix - a solution for sustainable development. Mater Today Proc. 2020 Jan;26:3250-6. https://doi.org/10.1016/j.matpr.2020.02.908
[15] Kumar R, Singh R, Patel M. Effect of metakaolin on mechanical characteristics of the mortar and concrete: A critical review. Mater Today Proc. 2023 Jan;93:315-9. https://doi.org/10.1016/j.matpr.2023.07.262
[16] Majhi RK, Nayak AN, Mukharjee BB. Development of sustainable concrete using recycled coarse aggregate and ground granulated blast furnace slag. Constr Build Mater. 2018 Jan;159:417-430. https://doi.org/10.1016/j.conbuildmat.2017.10.118
[17] Zeng Q, Li K. Reaction and microstructure of cement-fly-ash system. Mater Struct. 2015 Jun;48(6):1703-16. https://doi.org/10.1617/s11527-014-0266-y
[18] Lothenbach B, Nonat A. Calcium silicate hydrates: Solid and liquid phase composition. Cem Concr Res. 2015 Dec;78:57-70. https://doi.org/10.1016/j.cemconres.2015.03.019
[19] Provis JL. Alkali-activated materials. Cem Concr Res. 2018 Dec;114:40-8. https://doi.org/10.1016/j.cemconres.2017.02.009
[20] Babu BC, Durgarani K. Experimental study on the utilization of construction and demolition waste of recycled aggregate with GGBS and I-Crete in pavement quality concrete. Res. Eng. Struct. Mater., 2024; 10(4): 1483-1504. http://dx.doi.org/10.17515/resm2024.87me1110rs
[21] Zhang J, Wang Q, Wang Z. Optimizing design of high strength cement matrix with supplementary cementitious materials. Constr Build Mater. 2016 Sep;120:123-36. https://doi.org/10.1016/j.conbuildmat.2016.05.100
[22] Ma J, Zhang H, Wang D, Wang H, Chen G. Rheological Properties of Cement Paste Containing Ground Fly Ash Based on Particle Morphology Analysis. Crystals. 2022 Apr;12(4):524. https://doi.org/10.3390/cryst12040524
[23] Şimşek O, Pourghadri Sefidehkhan H, Gökçe HS. Performance of fly ash-blended Portland cement concrete developed by using fine or coarse recycled concrete aggregate. Constr Build Mater. 2022 Nov;357:129431. https://doi.org/10.1016/j.conbuildmat.2022.129431
[24] Ogirigbo OR, Black L. Influence of slag composition and temperature on the hydration and microstructure of slag blended cements. Constr Build Mater. 2016 Nov;126:496-507. https://doi.org/10.1016/j.conbuildmat.2016.09.057
[25] Wang J, Ng PL, Wang W, Du J, Song J. Modelling chloride diffusion in concrete with influence of concrete stress state. J Civ Eng Manag. 2017 Oct;23(7):955-65. https://doi.org/10.3846/13923730.2017.1343203
[26] Ramezanianpour AA, Pourkhorshidi AR, Sobhani J, Moodi F. Durability of concrete containing blended cements in harsh marine environments: 18 years exposure study. Constr Build Mater. 2021 Sep;299:123863. https://doi.org/10.1016/j.conbuildmat.2021.123863
[27] Lothenbach B, Scrivener K, Hooton RD. Supplementary cementitious materials. Cem Concr Res. 2011 Dec;41(12):1244-56. https://doi.org/10.1016/j.cemconres.2010.12.001
[28] Fang Z, Luo Luo Y, Chen H, Gao Y, Yang W, Wang C. Research on mechanical properties and hydration characteristics of ultra-high performance concrete with high-volume fly ash microsphere. J Build Eng. 2023 Nov;78:107738. https://doi.org/10.1016/j.jobe.2023.107738
[29] Hemalatha T, Sasmal S. Early-Age strength development in fly ash blended cement composites: Investigation through chemical activation. Mag Concr Res. 2019 Mar;71(5):260-70. https://doi.org/10.1680/jmacr.17.00336
[30] Briki Y, Zajac M, Ben Haha M, Scrivener K. Impact of limestone fineness on cement hydration at early age. Cem Concr Res. 2021 Sep;147:106515. https://doi.org/10.1016/j.cemconres.2021.106515
[31] Moula S, Ben Fraj A, Wattez T, Bouasker M, Bel Hadj Ali N. The very early-age behaviour of Ultra-High Performance Concrete containing ground granulated blast furnace slag. Constr Build Mater. 2023 Oct;400:132630. https://doi.org/10.1016/j.conbuildmat.2023.132630
[32] Bureau of Indian Standards. IS 456 (2000): Plain and Reinforced Concrete - Code of Practice. New Delhi: BIS; 2000.
[33] Wang XY. Analysis of hydration and strength optimization of cement-fly ash-limestone ternary blended concrete. Constr Build Mater. 2018 Mar;166:130-40. https://doi.org/10.1016/j.conbuildmat.2018.01.058
[34] Babalola OE, et al. Mechanical and durability properties of recycled aggregate concrete with ternary binder system and optimized mix proportion. J Mater Res Technol. 2020 May;9(3):6521-32. https://doi.org/10.1016/j.jmrt.2020.04.038
[35] Harish B, Dakshinamurthy NR, Sridhar M, Rao KJ. A study on mechanical properties of high strength concrete with alccofine as partial replacement of cement. Mater Today Proc. 2022 Jan;52:1201-10. https://doi.org/10.1016/j.matpr.2021.11.037

[36] Srinath BLNS, Patnaikuni CK, Balaji KVGD, Kumar BS, Manjunatha M. A prospective review of alccofine as supplementary cementitious material. Mater Today Proc. 2021 Jan;47:3953-9. https://doi.org/10.1016/j.matpr.2021.03.719
[37] Harish B, Dakshinamurthy NR, Sridhar M, Rao KJ. A study on mechanical properties of high strength concrete with Alccofine as partial replacement of cement. Materials Today: Proceedings. 2022;52:1201–1210.DOI: https://doi.org/10.1016/j.matpr.2021.11.037.
[38] Corbu O, Puskas A, Dragomir ML, Har N, Toma IO. Eco-Innovative Concrete for Infrastructure Obtained with Alternative Aggregates and a Supplementary Cementitious Material (SCM). Coatings. 2023 Oct;13(10):1710. https://doi.org/10.3390/coatings13101710
[39] Wang F, Kong X, Jiang L, Wang D. The acceleration mechanism of nano-C-S-H particles on OPC hydration. Constr Build Mater. 2020 Jul;249:118734. https://doi.org/10.1016/j.conbuildmat.2020.118734
[40] Amiri M, Aryanpour M, Porhonar F. Microstructural study of concrete performance after exposure to elevated temperatures via considering C-S-H nanostructure changes. High Temp Mater Proc. 2022 Jan;41(1):224-37. https://doi.org/10.1515/htmp-2022-0030
[41] Gao S, Guo X, Ban Y, Ma Y, Yu Q, Sui S. Influence of supplementary cementitious materials on ITZ characteristics of recycled concrete. Constr Build Mater. 2023 Jan;363:129736. https://doi.org/10.1016/j.conbuildmat.2022.129736
[42] Shamanth Gowda T, Ranganath RV. High early strength-high performance concrete produced with combination of ultra-fine slag and ultra-fine silica: Influence on fresh, mechanical, shrinkage and durability properties with microstructural investigation. Constr Build Mater. 2023 Jul;385:131462. https://doi.org/10.1016/j.conbuildmat.2023.131462
[43] Babalola OE et al. Mechanical and durability properties of recycled aggregate concrete with ternary binder system and optimized mix proportion. Journal of Materials Research and Technology. 2020;9(3):6521–6532. DOI: https://doi.org/10.1016/j.jmrt.2020.04.038
[44] Supit SWM, Shaikh FUA. Durability properties of high volume fly ash concrete containing nano-silica. Mater Struct. 2015 Aug;48(8):2431-45. https://doi.org/10.1617/s11527-014-0329-0
[45] Berodier E, Scrivener K. Development of pore structure, moisture sorption and transport properties in fly ash blended cement-based materials. Constr Build Mater. 2020 Nov;261:120007. https://doi.org/10.1016/j.conbuildmat.2020.120007
[46] Suda VBR, Priyatham Paul S. Relationship between compressive, split tensile and flexural strengths of ternary blended concrete. Mater Today Proc. 2022 Jan;65:1112-9. https://doi.org/10.1016/j.matpr.2022.04.162
[47] Fibre Reinforced Cementitious Composites. [Kitap/Kaynak detayları eksik].
[48] Lai MH, Lin JL, Cui J, Ren FM, Kitipornchai S, Ho JCM. A novel packing-coupled stress-strain model for confined concrete. Eng Struct. 2024 Mar;303(1):117415. https://doi.org/10.1016/j.engstruct.2023.117415
[49] Egan MD. Architectural acoustics. J. Ross Publishing; 2007.
[50] Zhang S, et al. Effect of Ultrafine Metakaolin on the Properties of Mortar and Concrete. Crystals. 2021;11(6):60. https://doi.org/10.3390/cryst11060665
[51] Tejakiran C, Kumar S K V S T L, Rani M S. Flexural behavior of ternary blended concrete beams with GFRP rebars strengthened with steel fiber and polypropylene fiber. Res. Eng. Struct. Mater., 2026; 12(1): 407-424. http://dx.doi.org/10.17515/resm2025-961me0612rs
[52] Ahmed M F. Enhancing the external sulfate attack resistance of high-volume fly ash concrete containing waste glass powder. Res. Eng. Struct. Mater., 2026; 12(2): 971-980. http://dx.doi.org/10.17515/resm2025-1267ic1015rs
[53] Sai V.H.; Lingeshwaran N.; Prasanna P.K.; George Fernandez Raj A.; Jayanthi P. Flexural behavior of GFRP rebars and steel rebars with polypropylene fibers and fly ash-based concrete. Research on Engineering Structures and Materials., 2025; 11(6): 3069-3085. https://jresm.org/article/resm2025-686me0214rs/.
[54] Tokala, Srinivasarao,; Lingeshwaran, N; Ponni, M; Ushakranti: J. George Fernandez Raj, A.; Chinnasamy, M. Recycling Construction and Demolition Waste into Coarse Aggregates: A State-of-the-Art Review, 2026: https://reference-global.com/download/article/10.2478/cee-2026-0059.pdf.
[55] Sai, Vudata Harsha; Lingeshwaran, N ; Pratheba, S. ; Lakshmi, B.V. Enhanced Mechanical and Flexural Performance of M40 Concrete with Hybrid Fibers and Fly Ash Replacement; 2025; Procedia Structural Integrity; 70, 509-516, https://www.sciencedirect.com/science/article/pii/S2452321625003142.
[56] Thurimella, Manoj Kumar; K J, Brahma Chari; N, Lingeshwaran; Raj A, George Fernandez; Singh, Rahul Kumar; Experimental investigation of structural behaviour and microstructural characteristics of steel fibre-reinforced concrete beams, Australian Journal of Structural Engineering, https://www.tandfonline.com/doi/abs/10.1080/13287982.2026.2643532,
[57] Babu K.V.; Chowdary C.H.M.; Lingeshwaran N.; Kishore I.S. Structural application of fiber reinforced concrete; 2025; Research on Engineering Structures and Materials, 11(6); 1913-1946; https://jresm.org/article/resm2024-305st0531rs/.

[58] Samanta S.; Lingeshwaran N; Synergistic Effects of Rice Husk Ash and Alccofine in Basalt Fiber Reinforced Concrete: A Comprehensive Review of Mechanical, Durability and Microstructural Performance; 2026; 8(2); 38-74; https://journals.asianresassoc.org/index.php/irjmt/article/view/5845.
[59] Bureau of Indian Standards. IS 3812-1 (2013): Specification for Pulverized Fuel Ash, Part 1: For Use as Pozzolana in Cement, Cement Mortar and Concrete. New Delhi: BIS; 2013.
[60] Bureau of Indian Standards. IS 12089 (1987): Specification for granulated slag for the manufacture of Portland slag cement. New Delhi: BIS; 1987.
[61] Bureau of Indian Standards. IS 10262:2019 - Concrete Mix Proportioning - Guidelines. New Delhi: BIS; 2019.
[62] Bureau of Indian Standards. IS 1199 (Part 2):2018 - Methods of Sampling and Analysis of Concrete. New Delhi: BIS; 2018.
[63] Bureau of Indian Standards. IS 516 (1959): Method of Tests for Strength of Concrete. New Delhi: BIS; 1959.
[64] Bureau of Indian Standards. IS 5816 (1999): Method of Test Splitting Tensile Strength of Concrete. New Delhi: BIS; 1999.
[65] Bureau of Indian Standards. IS 456 (2000): Plain and Reinforced Concrete - Code of Practice. New Delhi: BIS; 2000.
[66] Bureau of Indian Standards. IS 456 (2000): Plain and Reinforced Concrete - Code of Practice. New Delhi: BIS; 2000.